Demonstrating Experimentally the Encoding and Dynamics of an Error-Correctable Logical Qubit on a Hyperfine-Coupled Nuclear Spin Qudit

Sumin Lim,[1] Mikhail V. Vaganov,[1] Junjie Liu,[1,2,*] and Arzhang Ardavan[1,†]

[1]*CAESR, Department of Physics, University of Oxford, The Clarendon Laboratory, Parks Road, Oxford OX1 3PU, United Kingdom*
[2]*School of Physical and Chemical Sciences, Queen Mary University of London, London E1 4NS, United Kingdom*

(Received 7 August 2024; revised 11 November 2024; accepted 9 January 2025; published 20 February 2025)

The realization of effective quantum error correction protocols remains a central challenge in the development of scalable quantum computers. Employing high-dimensional quantum systems (qudits) can offer more hardware-efficient protocols than qubit-based approaches. Using electron-nuclear double resonance, we implement a logical qubit encoded on the four states of a $I = 3/2$ nuclear spin hyperfine-coupled to an $S = 1/2$ electron spin qubit; the encoding protects against the dominant decoherence mechanism in such systems, i.e., fluctuations of the quantizing magnetic field. We explore the dynamics of the encoded state both under a controlled application of the fluctuation and under natural decoherence processes. Our results confirm the potential of these proposals for practical, implementable, fault-tolerant quantum memories.

DOI: 10.1103/PhysRevLett.134.070603

While the control fidelity in few-qubit systems has reached two or three nines [1–4], maintaining this becomes increasingly difficult as the size of the system is scaled up to tens of qubits [5,6]. Regardless of the physical platform, unwanted interqubit interactions and coupling to the environment drastically reduce the overall fidelity of the quantum computing system. Quantum error correction protocols seek to address these challenges by enlarging the Hilbert space to store information with redundancy [7,8]. Many current proposals are based on the idea of using multiple physical qubits to encode an individual logical qubit [9–12], yielding qubit-based error correction algorithms such as surface codes [13,14]. An alternative paradigm deploys arbitrary d-dimensional quantum systems (where $d > 2$), known as qudits. This approach reduces the overhead associated with additional qubits, and can provide a hardware-efficient structure. Originally proposed by Gottesman, Kitaev, and Preskill [15], a range of theoretical [16–19] and experimental [20–25] explorations are ongoing into systems based on quantum harmonic oscillators with bosonic eigenstates. This kind of approach provides infinite dimensions in a spatially compact system, but at the cost of complexity in practical operations.

In this context, quantum spins greater than $1/2$ offer a promising alternative: a single physical object providing a multidimensional but finite and, often, well-isolated Hilbert space. Electronic spins in condensed matter, with their well-defined quantum properties and relatively weak interactions with external excitations, are natural candidates for embodying quantum information; their hyperfine-coupled nuclear spins, which tend to be even more coherent, offer potential as quantum memory elements. Indeed, such systems featured among the earliest theoretical condensed matter quantum information proposals such as that of Kane [26], and various physical examples have been studied experimentally, including paramagnetic defects in semiconductors [27–29] and diamond [30–33] and molecular magnets [34,35]. Together, these observations motivate us to explore how a nuclear spin qudit hyperfine-coupled to an electron spin qubit [36–41] can be used to encode fault-tolerant error correcting protocols [42–44].

A particularly simple proposal employs an electron spin $S = 1/2$ hyperfine-coupled to a nuclear spin $I = 3/2$ to encode logical qubit states protected against fluctuations of the magnetic field ΔB_z along the quantization axis, represented by

$$\hat{O}_{\mathrm{fluc}} = (\gamma_{\mathrm{S}}\hat{S}_z + \gamma_{\mathrm{I}}\hat{I}_z)\Delta B_z, \tag{1}$$

where γ_{S} and γ_{I} are the electron and nuclear spin gyromagnetic ratios respectively. A qubit state $|\psi\rangle$ encoded on the electron spin with a particular projection of the nuclear spin can be represented in the notation $|m_S\rangle \otimes |m_I\rangle$ as

$$|\psi\rangle = \left(\alpha\left|-\frac{1}{2}\right\rangle + \beta\left|+\frac{1}{2}\right\rangle\right) \otimes \left|-\frac{1}{2}\right\rangle \tag{2}$$

where α and β are, in general, complex. This state is rotated to the protected "encoded" state

[*]Contact author: junjie.liu@qmul.ac.uk
[†]Contact author: arzhang.ardavan@physics.ox.ac.uk

$$|\psi_L\rangle = \alpha|0_L\rangle + \beta|1_L\rangle, \tag{3}$$

where

$$|0_L\rangle = \left|-\frac{1}{2}\right\rangle \otimes \left(\frac{1}{2}\left|-\frac{3}{2}\right\rangle + \frac{\sqrt{3}}{2}\left|+\frac{1}{2}\right\rangle\right),$$
$$|1_L\rangle = \left|-\frac{1}{2}\right\rangle \otimes \left(\frac{1}{2}\left|+\frac{3}{2}\right\rangle + \frac{\sqrt{3}}{2}\left|-\frac{1}{2}\right\rangle\right). \tag{4}$$

The logical states $|0_L\rangle$ and $|1_L\rangle$ are chosen such that they and the states connected by the perturbation against which we wish to protect (i.e., $\hat{O}_{\rm fluc}|0_L\rangle$ and $\hat{O}_{\rm fluc}|1_L\rangle$) form a mutually orthogonal set of states. Note that the electron spin parts of $|0_L\rangle$ and $|1_L\rangle$ are eigenstates of $\widehat{S}_z$ with the same m_S; because $\gamma_{\rm S}$ is generally larger than $\gamma_{\rm I}$, encoding the qubit in the nuclear degrees of freedom already provides an element of protection against magnetic field fluctuations [27]. The result of the magnetic field fluctuation acting for time δt on the logical qubit state is therefore

$$\exp\left(-\frac{\mathrm{i}}{\hbar}\hat{O}_{\rm fluc}\delta t\right)|\psi_L\rangle = \exp\left(\mathrm{i}\frac{\omega_S}{2}\delta t\right)\exp\left(-\mathrm{i}\theta\widehat{I}_z\right)|\psi_L\rangle, \tag{5}$$

where $\omega_S = \gamma_S \Delta B_z$ and $\theta = \gamma_I \Delta B_z \delta t/\hbar$. The first factor is an overall phase that is undetectable for this system in isolation; we shall neglect it in what follows. Expanding the second factor,

$$\exp\left(-\mathrm{i}\theta\widehat{I}_z\right)|\psi_L\rangle = \sum_n A_n \frac{(-\mathrm{i}\theta)^n}{n!}\widehat{I}_z^{\,n}|\psi_L\rangle$$
$$\approx A_0|\psi_L\rangle - \mathrm{i}A_1\theta\widehat{I}_z|\psi_L\rangle, \tag{6}$$

where the approximation holds for a weak perturbation, i.e., a small ΔB_z acting for a short time δt. The effect of the perturbation is to shift amplitude from the logical qubit subspace into the (by construction) orthogonal "error" subspace spanned by $\widehat{I}_z|0_L\rangle$ and $\widehat{I}_z|1_L\rangle$. Here, $A_n = 1$ for all n; we shall later use A_n to parametrize our experimental results.

The fact that the uncorrupted component [the first term in Eq. (6)] is orthogonal to the corrupted component (the second term) allows us to identify a unitary transformation (see Supplemental Material [45], Sec. I) "decoding" [43] this state to

$$A_0\left|-\frac{1}{2}\right\rangle \otimes \left(\alpha\left|-\frac{1}{2}\right\rangle + \beta\left|+\frac{1}{2}\right\rangle\right)$$
$$- \mathrm{i}A_1\theta\left|+\frac{1}{2}\right\rangle \otimes \left(\alpha\left|-\frac{1}{2}\right\rangle + \beta\left|+\frac{1}{2}\right\rangle\right). \tag{7}$$

Thus, a projective measurement of the electron spin state m_S yields whether an error occurred ($m_S = +1/2$) or not ($m_S = -1/2$); in either case, the error-corrected qubit state is recovered on an $m_I = \pm 1/2$ superposition.

There are certain requirements on a physical system on which this protocol is to be implemented. From the fundamental perspective, we require that $S \geq 1/2$ and $I \geq 3/2$, that all transitions are independently spectrally addressable, and the availability of projective measurement of the electron spin.

While a number of physical systems show promise in meeting these requirements [34,46,47], we have chosen to explore the implementation and spin dynamics of the protocol in a system offering experimental convenience and flexibility at the cost of the availability of projective measurement.

Manganese defects (Mn^{2+}, atomic configuration [Ar]$3d^5 4s^0$) in single-crystal Wurtzite zinc oxide (ZnO) offer a homogeneous ensemble of highly coherent electronic spins with $S = 5/2$, each hyperfine-coupled to the ^{55}Mn nuclear spin $I = 5/2$, yielding a spin Hilbert space of dimension 36. We can conveniently control the electron-nuclear spin system using electron and nuclear pulsed magnetic resonance, and detect ensemble electron spin coherences via Hahn echoes. The experiment reported here does not require additional optical excitation or readout processes [30–33,48].

The electron spin resonance (ESR) and electron-nuclear double resonance (ENDOR) spectra of Mn:ZnO have been studied extensively [49–51]. For a magnetic field B_z aligned along the crystal c axis, the low-energy spin degrees of freedom are described well by the Hamiltonian

$$H = (\gamma_S\widehat{S}_z + \gamma_I\widehat{I}_z)B_z + A_{\rm h.f.}\hat{\mathbf{S}}\cdot\hat{\mathbf{I}} - D\widehat{S}_z^{\,2} \tag{8}$$

comprising electron and nuclear spin Zeeman terms, an isotropic hyperfine coupling, and an electron spin zero-field splitting. In units convenient for understanding the experiment, $\gamma_S/h \approx 28.02$ GHz/T, $\gamma_I/h \approx -10.96$ MHz/T, $A_{\rm h.f.}/h \approx -220.0$ MHz, and $D/h \approx 707.0$ MHz, yielding an energy level structure shown as a function of magnetic field in Fig. 1(a). The electron spin coherence time T_{2e} is about 80 μs below 30 K and approaches a millisecond below 10 K [50] (see Supplemental Material, Sec. II). The electron spin zero-field splitting ensures that the six allowed ESR transitions (for which $\Delta m_S = \pm 1$) are non-degenerate. The A_{xx} and A_{yy} terms in the isotropic hyperfine interaction lead to second-order shifts in the nuclear spin energy levels of order $A_{\rm h.f.}^2/\gamma_S B_z$, which for an electron spin Zeeman frequency in X band (∼9.7 GHz, corresponding to $B_z \sim 0.35$ T) lifts the degeneracy of the allowed NMR transitions ($\Delta m_I = \pm 1$) by about 4 MHz. Thus, owing to the final two terms in the Hamiltonian, Eq. (8), all of the spin transitions occur at distinct frequencies and are spectrally addressable (see Supplemental Material, Secs. III and IV).

In this Letter, we exploit this addressability to select the subspace suitable for implementation of the fault-tolerant memory protocol described above. In fact, the encoding in Eqs. (2)–(4) and the experiments described below involve only one level from the $m_S = +1/2$ subspace, $|+1/2\rangle \otimes |-1/2\rangle$, in addition to the four levels in the

$m_S = -1/2$ subspace, $|-1/2\rangle \otimes |m_I\rangle$ with $m_I = -3/2, -1/2, +1/2, +3/2$. In our finite-temperature ensemble experiment, this approach provides an important practical advantage: the electronic Zeeman energy is significantly larger than the nuclear state energy splittings in the $m_S = -1/2$ subspace, so our thermal state is effectively a pseudopure state, not requiring active preparation [52,53] (see Supplemental Material, Sec. V). A further practical reason for working within the $m_S = \pm 1/2$ subspace is that these levels are unaffected by the dominant inhomogeneous broadening mechanism in this material, which is the strain in the zero-field splitting parameter D in Eq. (8) [50].

We mounted a Mn doped ZnO single crystal of dimensions of 2.5 mm × 6 mm × 0.5 mm in a Bruker MD4 resonator with the crystal c axis parallel to the external magnetic field. We measured ESR and ENDOR spectra at 30 K (elevated from the base temperature so as to limit T_{1n} and therefore increase the available experimental shot repetition rate) using an X-band (∼9.7 GHz) home-built spectrometer. Through ESR [Fig. 1(b)] and ENDOR [Fig. 1(d)] spectroscopies, we obtained the frequencies of the transitions within the relevant subspace. Subsequent coherence transfer experiments between the electronic and nuclear degrees of freedom [27,54,55] and within the nuclear spin qudit subspace confirmed that quantum information can be generated, encoded, and read out in the electron-nuclear coupled system (see Supplemental Material, Secs. III and IV). The fidelities of the relevant microwave and rf pulses are estimated [56] to be $99.5 \pm 0.1\%$ and $93.5 \pm 0.1\%$, with details provided in Supplemental Material, Sec. VI.

The coherence transfer experiments equip us to implement the encoding defined in Eqs. (3) and (4), and to explore the dynamics of the encoded state. Figure 2(a) shows the pulse sequence on which our investigation is based; it comprises four units. The first, the encoding unit labeled "ENC," generates an electron spin qubit state (chosen as $\alpha = \beta = 1/\sqrt{2}$, i.e., a $\widehat{\sigma_x}$ eigenstate) and then transfers it to the logical states defined in Eqs. (3) and (4).

This is followed by a controlled application of the perturbation against which the encoding is designed to protect, a fluctuation of B_z, in a unit of the sequence labeled "$\widehat{Z(\theta)}$." We achieve this by applying a current pulse of calibrated amplitude and duration to a pair of appropriately oriented Helmholtz coils proximal to the sample (see Supplemental Material, Sec. VII). With small currents

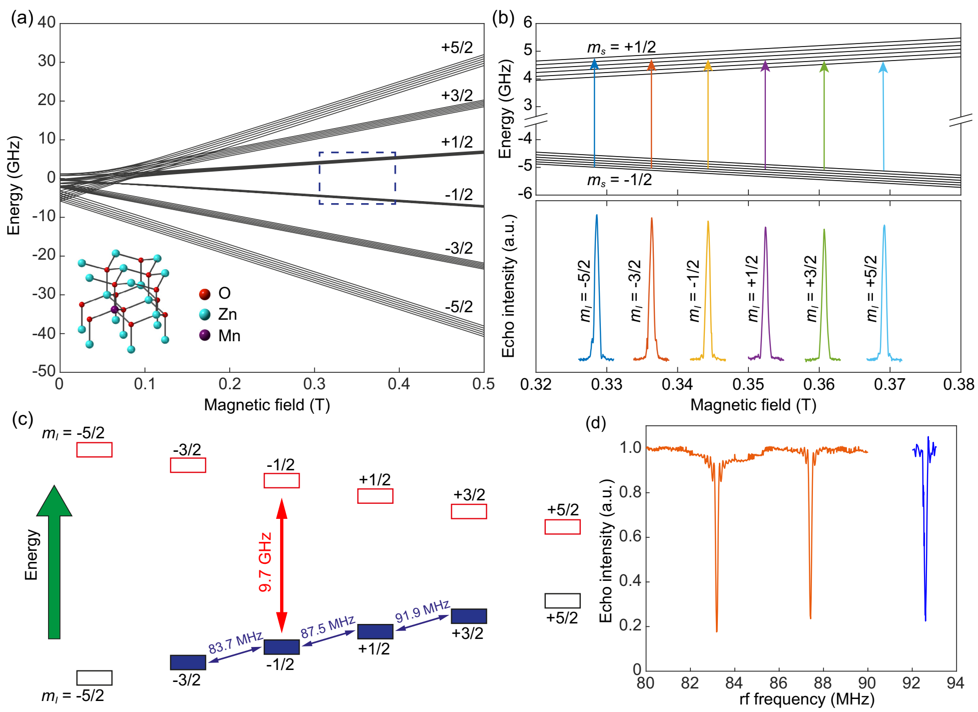

FIG. 1. ESR and ENDOR spectroscopy at a temperature of 30 K where the electronic $T_{1e} \approx 1.3$ ms. (a) The spin energy levels of Mn^{2+} defects in ZnO. Inset: the atomic structure of the defect. (b) Echo-detected field swept ESR spectra at 9.7 GHz, showing the six $|-1/2, m_I\rangle$ to $|1/2, m_I\rangle$ ESR transitions corresponding to each m_I projection. (c) Owing to the second order hyperfine shifts, the nuclear spin transitions within $m_S = -1/2$ are nondegenerate and therefore spectrally addressable. (d) Davies ENDOR spectra obtained at 0.3443 T. The two peaks at 83.7 and 87.5 MHz (orange) correspond to transitions from $|-1/2, -1/2\rangle$ to $|-1/2, -3/2\rangle$ and to $|-1/2, +1/2\rangle$, respectively. The peak at 92.6 MHz, corresponding to the transition from $|-1/2, +1/2\rangle$ to $|-1/2, +3/2\rangle$, is obtained from a modified Davies ENDOR sequence including a rf π pulse at 87.5 MHz before the frequency-swept rf pulse, as described in Sec. III of the Supplemental Material.

applied for short durations, the effect of the artificial perturbation is small and the approximation in Eq. (6) holds. By increasing the current and the pulse duration, we have the scope to explore experimentally the regime beyond the small-perturbation limit; our apparatus allows us to apply pulses for which θ exceeds $\pm\pi/2$ radians.

Working with an ensemble introduces a requirement that we account for inhomogeneities. In the qubit case, where only two energy eigenstates are involved in a superposition, the effects of static inhomogeneities are refocused by a single π pulse. In our qudit case, involving a superposition across four energy eigenstates, the situation is more subtle; it is not straightforward to implement an operation achieving full refocusing while preserving the system within the error-protected subspace. (Approaches to refocusing arbitrary qudit states have been identified [57], but they lead to extended periods when the encoded state resides outside the logical qubit space, destroying the protection.) Under this constraint it is only possible to guarantee refocusing within the $m_I = \pm 3/2$ and $m_I = \pm 1/2$ subspaces, but the relative phase between these subspaces is uncontrolled. This refocusing is achieved by the third unit in the sequence, comprising eight π pulses and labeled “REF” (see Supplemental Material, Sec. VIII).

The experiment therefore yields, as a function of the artificially applied error angle θ, four echoes: the in-phase (x) and out-of-phase (y) components of echoes arising from the $m_I = +1/2, -1/2$ [obtained with the green pulses in Fig. 2(a) absent] and the $m_I = +3/2, -3/2$ coherences (obtained with the green pulses present). We label the echo amplitudes $I_{\pm\frac{1}{2},x}$, $I_{\pm\frac{1}{2},y}$, $I_{\pm\frac{3}{2},x}$, $I_{\pm\frac{3}{2},y}$. These are plotted in Fig. 2(b) as points for a fixed storage time of 0.1 ms. They are accompanied by a global fit to a model based on a truncation of the series in Eq. (6) with free parameters A_n, $n = 0 \ldots 5$ (solid lines). Also shown are the amplitudes expected under the exact theoretical evolution with θ (dashed lines). The values of the fit parameters are given in Table I normalized to A_0, accounting for the overall echo signal gain in the experiment. The proximity of A_n/A_0 (with $n > 0$) to 1 is indicative of how close the evolution of the system is to the exact theoretical evolution.

Given that we cannot achieve full refocusing and that our detection of the properties of the system state is via Hahn echoes of electron spin coherences, this question arises: what features of the protected state can we observe as a function of the perturbation $\widehat{Z(\theta)}$? The echo amplitudes can be expressed in terms of A_n as

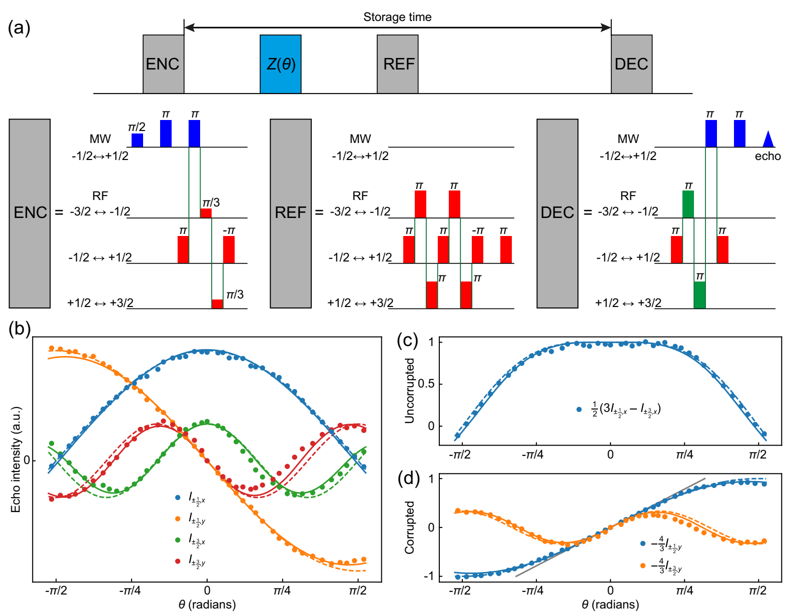

FIG. 2. Implementation and evolution of the error-protected state. (a) The pulse sequence comprising “ENC,” the generation of a qubit state and its encoding in the logical-qubit subspace; “$\widehat{Z(\theta)}$,” the controlled artificial perturbation; “REF,” refocusing the inhomogeneities within the nuclear subspace; “DEC,” decoding pulses allowing measurement of the nuclear coherences $m_I = -1/2, +1/2$ (green pulses absent) and $m_I = -3/2, +3/2$ (green pulses present). All microwave (MW) pulses are resonant with the $m_S = \pm 1/2$ transition for the $m_I = -1/2$ nuclear spin projection. All rf pulses are within the $m_S = -1/2$ subspace. (b) The evolution of the four detectable echoes at the end of the sequence as a function of the applied perturbation angle θ with a fixed storage time of 0.1 ms. (c) A linear combination of the echoes yielding, for small θ, the squared amplitude of the uncorrupted component A_0^2. (d) Rescaled appropriately, the out-of-phase echoes yield the amplitude of the corrupted component for small θ. The gray line has gradient 1 and passes through the origin. In (b), (c), and (d), points are data; solid lines represent the global fit to a model with six parameters, $A_0, \ldots, A_5$, as defined in Eq. (6); dashed lines represent the ideal exact evolution of the system with the only parameter being the overall vertical scale.

TABLE I. Values of the fit parameters A_n. They are normalized to A_0, which defines the overall vertical scale in Fig. 2(b). Quoted errors are $\pm 1\sigma$ bounds.

A_0	A_1/A_0	A_2/A_0	A_3/A_0	A_4/A_0	A_5/A_0
14.19 $\pm$0.05	0.997 $\pm$0.008	1.12 $\pm$0.02	1.13 $\pm$0.05	1.02 $\pm$0.05	1.2 $\pm$0.2

$$
\begin{aligned}
I_{\pm\frac{1}{2},x} &= \frac{3}{4}A_0^2 - \frac{3\theta^2}{16}(A_1^2 + A_0A_2) + O(\theta^4) \\
I_{\pm\frac{1}{2},y} &= -\frac{3\theta}{4}A_0A_1 + \frac{\theta^3}{32}(3A_1A_2 + A_0A_3) + O(\theta^5) \\
I_{\pm\frac{3}{2},x} &= \frac{1}{4}A_0^2 - \frac{9\theta^2}{16}(A_1^2 + A_0A_2) + O(\theta^4) \\
I_{\pm\frac{3}{2},y} &= -\frac{3\theta}{4}A_0A_1 + \frac{9\theta^3}{32}(3A_1A_2 + A_0A_3) + O(\theta^5). \qquad (9)
\end{aligned}
$$

(We note here that if we had chosen our original qubit to be an eigenstate of $\widehat{\sigma_y}$, the x and y components of these echoes would be exchanged.)

Our principal experimental objective is to monitor the evolution of state amplitude from the logical qubit subspace into the orthogonal "error" subspace defined immediately following Eq. (6) under the action of the perturbation, i.e., to monitor the amplitudes A_0 and $A_1\theta$ as a function of θ. We can access these quantities from the available echo data. The linear combination

$$\frac{3I_{\pm\frac{1}{2},x} - I_{\pm\frac{3}{2},x}}{2} = A_0^2 + O(\theta^4) \qquad (10)$$

yields the square of the uncorrupted amplitude, and is plotted in Fig. 2(c) as a function of θ (points), along with the model fit (solid line) and the predicted exact evolution (dashed line). The remarkably flat behavior over a wide range around $\theta = 0$ is a direct reflection of the fact that the perturbation is moving amplitude from the logical qubit subspace into an orthogonal subspace. We may obtain the amplitude of the corrupted state directly from a scaling of the out-of-phase echoes

$$
\begin{aligned}
-\frac{4I_{\pm\frac{1}{2},y}}{3} &= A_0A_1\theta + O(\theta^3) \\
-\frac{4I_{\pm\frac{3}{2},y}}{3} &= A_0A_1\theta + O(\theta^3) \qquad (11)
\end{aligned}
$$

as plotted in Fig. 2(d). Over a significant range around $\theta = 0$, both quantities are coincident with a line of gradient 1 through the origin, confirming that they faithfully report the corrupted amplitude.

Given the coincidence of $T_{2\mathrm{n}}$ and $T_{1\mathrm{e}}$ obtained from coherence transfer experiments (see Supplemental Material, Sec. III), we expect the dominant natural decoherence process affecting the nuclear spin to be fluctuations of the magnetic field along the quantization axis arising from electron spin flips coupled through the diagonal component of the hyperfine interaction. It is therefore interesting to explore the behavior of the encoded state under the action of the natural decoherence processes present in the system, i.e., as a function of the storage time without the application of the artificial perturbation.

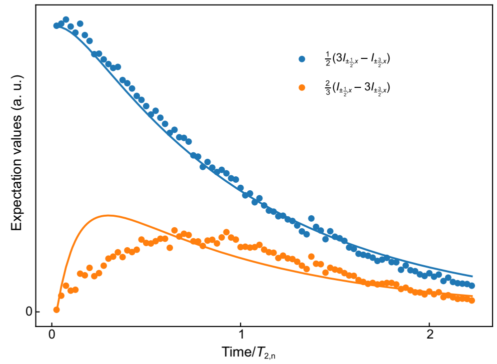

FIG. 3. Evolution of the encoded state with natural decoherence. Points are the amplitude squared of the uncorrupted component [Eq. (10), blue)] and the quantity related to the squared amplitude of the corrupted component [Eq. (12), orange]. Lines correspond to a minimal master equation model incorporating only $\widehat{I_z}$ as a relaxation operator.

In contrast to our artificial perturbation operation $\widehat{Z(\theta)}$, natural processes affect each member of the ensemble independently and incoherently. This means that for our choice of qubit state all out-of-phase echo components are zero and we cannot monitor the corrupted amplitude using the strategy in Eq. (11). Instead, we construct a linear combination from the in-phase echoes

$$\frac{2(I_{\pm\frac{1}{2},x} - 3I_{\pm\frac{3}{2},x})}{3} = (A_1^2 + A_0A_2)\theta^2, \qquad (12)$$

which gives us a quantity related to the square of the amplitude of the corrupted component.

In Fig. 3 we plot this quantity and the square of the uncorrupted amplitude [Eq. (10)] as a function of the storage time [defined in Fig. 2(a)] without applying the artificial perturbation $\widehat{Z(\theta)}$. At short times (below $\sim 0.1T_{2\mathrm{n}}$) the uncorrupted component is approximately independent of time, after which it falls approximately exponentially with a timescale characteristic of $T_{2\mathrm{n}}$. The corrupted component starts at zero and increases linearly at short times, eventually decaying at longer times also on the $T_{2\mathrm{n}}$ timescale. This behavior is consistent with our logical qubit state being orthogonal to the state to which the dominant phase relaxation process mixes. The solid lines in Fig. 3 represent the predictions of a minimal Lindblad master equation model with the relaxation operator $\sqrt{2/T_{2\mathrm{n}}}\widehat{I_z}$ determined from an independent measurement of $T_{2\mathrm{n}}$; the only free parameter is the vertical scaling. This model describes the qualitative behavior well.

The results presented in Figs. 2 and 3 offer strong evidence that we can implement the logical qubit encoding presented in Eq. (4), and that its dynamics under the perturbation that it is designed to protect against are as expected. We conclude that the deployment of hyperfine-coupled nuclear qudits can indeed offer a valuable resource for implementing fault-tolerant quantum memories [42–44]. The potential of this approach provides fresh impetus for developing single-spin, single-shot projective measurement for condensed matter based electron spin qubits, including broadening the scope of applicability of demonstrated methods [34,35] as well as exploring new approaches. The important question of the potential performance of a quantum memory of the kind described here is explored elsewhere [43], but we note that it will depend critically on the fidelities of both the encoding and measurement protocols.

Acknowledgments—This project has received funding from the European Union's Horizon 2020 research and innovation programme under Grant Agreements No. 862893 (FATMOLS) and No. 863098 (SPRING). J. L. acknowledges support from the Royal Society under grant URF\R1\201132. M. V. is grateful to the Hill Foundation for financial support.

[1] A. Noiri, K. Takeda, T. Nakajima, T. Kobayashi, A. Sammak, G. Scappucci, and S. Tarucha, Fast universal quantum gate above the fault-tolerance threshold in silicon, Nature (London) **601**, 338 (2022).
[2] X. Xue, M. Russ, N. Samkharadze, B. Undseth, A. Sammak, G. Scappucci, and L. M. Vandersypen, Quantum logic with spin qubits crossing the surface code threshold, Nature (London) **601**, 343 (2022).
[3] J. Yoneda, K. Takeda, T. Otsuka, T. Nakajima, M. R. Delbecq, G. Allison, T. Honda, T. Kodera, S. Oda, Y. Hoshi *et al.*, A quantum-dot spin qubit with coherence limited by charge noise and fidelity higher than 99.9%, Nat. Nanotechnol. **13**, 102 (2018).
[4] C. Yang, K. Chan, R. Harper, W. Huang, T. Evans, J. Hwang, B. Hensen, A. Laucht, T. Tanttu, F. Hudson *et al.*, Silicon qubit fidelities approaching incoherent noise limits via pulse engineering, Nat. Electron. **2**, 151 (2019).
[5] J. Preskill, Quantum computing 40 years later, arXiv:2106.10522.
[6] J. Preskill, Quantum computing in the NISQ era and beyond, Quantum **2**, 79 (2018).
[7] B. M. Terhal, Quantum error correction for quantum memories, Rev. Mod. Phys. **87**, 307 (2015).
[8] D. Gottesman, *Stabilizer Codes and Quantum Error Correction* (California Institute of Technology, Pasadena, CA, 1997).
[9] D. P. DiVincenzo and P. W. Shor, Fault-tolerant error correction with efficient quantum codes, Phys. Rev. Lett. **77**, 3260 (1996).
[10] R. Laflamme, C. Miquel, J. P. Paz, and W. H. Zurek, Perfect quantum error correcting code, Phys. Rev. Lett. **77**, 198 (1996).
[11] E. Knill and R. Laflamme, Theory of quantum error-correcting codes, Phys. Rev. A **55**, 900 (1997).
[12] E. Knill, R. Laflamme, and L. Viola, Theory of quantum error correction for general noise, Phys. Rev. Lett. **84**, 2525 (2000).
[13] E. Dennis, A. Kitaev, A. Landahl, and J. Preskill, Topological quantum memory, J. Math. Phys. (N.Y.) **43**, 4452 (2002).
[14] Z. Chen, K. J. Satzinger, J. Atalaya, A. N. Korotkov, A. Dunsworth, D. Sank, C. Quintana, M. McEwen, R. Barends, P. V. Klimov *et al.*, Exponential suppression of bit or phase errors with cyclic error correction, Nature (London) **595**, 383 (2021).
[15] D. Gottesman, A. Kitaev, and J. Preskill, Encoding a qubit in an oscillator, Phys. Rev. A **64**, 012310 (2001).
[16] S. Pirandola, S. Mancini, S. L. Braunstein, and D. Vitali, Minimal qudit code for a qubit in the phase-damping channel, Phys. Rev. A **77**, 032309 (2008).
[17] K. Noh, S. M. Girvin, and L. Jiang, Encoding an oscillator into many oscillators, Phys. Rev. Lett. **125**, 080503 (2020).
[18] V. V. Albert, J. P. Covey, and J. Preskill, Robust encoding of a qubit in a molecule, Phys. Rev. X **10**, 031050 (2020).
[19] B. Royer, S. Singh, and S. M. Girvin, Stabilization of finite-energy Gottesman-Kitaev-Preskill states, Phys. Rev. Lett. **125**, 260509 (2020).
[20] L. Hu, Y. Ma, W. Cai, X. Mu, Y. Xu, W. Wang, Y. Wu, H. Wang, Y. Song, C.-L. Zou *et al.*, Quantum error correction and universal gate set operation on a binomial bosonic logical qubit, Nat. Phys. **15**, 503 (2019).
[21] C. Flühmann and J. P. Home, Direct characteristic-function tomography of quantum states of the trapped-ion motional oscillator, Phys. Rev. Lett. **125**, 043602 (2020).
[22] N. Ofek, A. Petrenko, R. Heeres, P. Reinhold, Z. Leghtas, B. Vlastakis, Y. Liu, L. Frunzio, S. Girvin, L. Jiang *et al.*, Extending the lifetime of a quantum bit with error correction in superconducting circuits, Nature (London) **536**, 441 (2016).
[23] P. Campagne-Ibarcq, A. Eickbusch, S. Touzard, E. Zalys-Geller, N. E. Frattini, V. V. Sivak, P. Reinhold, S. Puri, S. Shankar, R. J. Schoelkopf *et al.*, Quantum error correction of a qubit encoded in grid states of an oscillator, Nature (London) **584**, 368 (2020).
[24] R. W. Heeres, P. Reinhold, N. Ofek, L. Frunzio, L. Jiang, M. H. Devoret, and R. J. Schoelkopf, Implementing a universal gate set on a logical qubit encoded in an oscillator, Nat. Commun. **8**, 1 (2017).
[25] J. M. Gertler, B. Baker, J. Li, S. Shirol, J. Koch, and C. Wang, Protecting a bosonic qubit with autonomous quantum error correction, Nature (London) **590**, 243 (2021).
[26] B. E. Kane, A silicon-based nuclear spin quantum computer, Nature (London) **393**, 133 (1998).
[27] J. J. Morton, A. M. Tyryshkin, R. M. Brown, S. Shankar, B. W. Lovett, A. Ardavan, T. Schenkel, E. E. Haller, J. W. Ager, and S. Lyon, Solid-state quantum memory using the 31P nuclear spin, Nature (London) **455**, 1085 (2008).
[28] A. Morello, J. J. Pla, F. A. Zwanenburg, K. W. Chan, K. Y. Tan, H. Huebl, M. Möttönen, C. D. Nugroho, C. Yang, J. A. van Donkelaar, A. D. C. Alves, D. N. Jamieson,

C. C. Escott, L. C. L. Hollenberg, R. G. Clark, and A. S. Dzurak, Single-shot readout of an electron spin in silicon, Nature (London) **467**, 687 (2010).

[29] J. J. Pla, K. Y. Tan, J. P. Dehollain, W. H. Lim, J. J. L. Morton, F. A. Zwanenburg, D. N. Jamieson, A. S. Dzurak, and A. Morello, High-fidelity readout and control of a nuclear spin qubit in silicon, Nature (London) **496**, 334 (2013).

[30] G. Waldherr, Y. Wang, S. Zaiser, M. Jamali, T. Schulte-Herbrüggen, H. Abe, T. Ohshima, J. Isoya, J. F. Du, P. Neumann, and J. Wrachtrup, Quantum error correction in a solid-state hybrid spin register, Nature (London) **506**, 204 (2014).

[31] T. H. Taminiau, J. Cramer, T. van der Sar, V. V. Dobrovitski, and R. Hanson, Universal control and error correction in multi-qubit spin registers in diamond, Nat. Nanotechnol. **9**, 171 (2014).

[32] L. Robledo, L. Childress, H. Bernien, B. Hensen, P. F. Alkemade, and R. Hanson, High-fidelity projective read-out of a solid-state spin quantum register, Nature (London) **477**, 574 (2011).

[33] C. E. Bradley, J. Randall, M. H. Abobeih, R. C. Berrevoets, M. J. Degen, M. A. Bakker, M. Markham, D. J. Twitchen, and T. H. Taminiau, A ten-qubit solid-state spin register with quantum memory up to one minute, Phys. Rev. X **9**, 031045 (2019).

[34] R. Vincent, S. Klyatskaya, M. Ruben, W. Wernsdorfer, and F. Balestro, Electronic read-out of a single nuclear spin using a molecular spin transistor, Nature (London) **488**, 357 (2012).

[35] S. Thiele, F. Balestro, R. Ballou, S. Klyatskaya, M. Ruben, and W. Wernsdorfer, Electrically driven nuclear spin resonance in single-molecule magnets, Science **344**, 1135 (2014).

[36] S. Asaad, V. Mourik, B. Joecker, M. A. Johnson, A. D. Baczewski, H. R. Firgau, M. T. Madzik, V. Schmitt, J. J. Pla, F. E. Hudson *et al.*, Coherent electrical control of a single high-spin nucleus in silicon, Nature (London) **579**, 205 (2020).

[37] I. Fernandez de Fuentes, T. Botzem, M. A. I. Johnson, A. Vaartjes, S. Asaad, V. Mourik, F. E. Hudson, K. M. Itoh, B. C. Johnson, A. M. Jakob, J. C. McCallum, D. N. Jamieson, A. S. Dzurak, and A. Morello, Navigating the 16-dimensional Hilbert space of a high-spin donor qudit with electric and magnetic fields, Nat. Commun. **15**, 1380 (2024).

[38] X. Yu, B. Wilhelm, D. Holmes, A. Vaartjes, D. Schwienbacher, M. Nurizzo, A. Kringhøj, M. R. van Blankenstein, A. M. Jakob, P. Gupta, F. E. Hudson, K. M. Itoh, R. J. Murray, R. Blume-Kohout, T. D. Ladd, A. S. Dzurak, B. C. Sanders, D. N. Jamieson, and A. Morello, Creation and manipulation of Schrödinger cat states of a nuclear spin qudit in silicon, arXiv:2405.15494.

[39] A. Chiesa, F. Petiziol, E. Macaluso, S. Wimberger, P. Santini, and S. Carretta, Embedded quantum-error correction and controlled-phase gate for molecular spin qubits, AIP Adv. **11**, 025134 (2021).

[40] J. A. Gross, C. Godfrin, A. Blais, and E. Dupont-Ferrier, Hardware-efficient error-correcting codes for large nuclear spins, Phys. Rev. Appl. **22**, 014006 (2024).

[41] S. Chicco, G. Allodi, A. Chiesa, E. Garlatti, C. D. Buch, P. Santini, R. De Renzi, S. Piligkos, and S. Carretta, Proof-of-concept quantum simulator based on molecular spin qudits, J. Am. Chem. Soc. **146**, 1053 (2023).

[42] J. A. Gross, Designing codes around interactions: The case of a spin, Phys. Rev. Lett. **127**, 010504 (2021).

[43] A. Chiesa, E. Macaluso, F. Petiziol, S. Wimberger, P. Santini, and S. Carretta, Molecular nanomagnets as qubits with embedded quantum-error correction, J. Phys. Chem. Lett. **11**, 8610 (2020).

[44] S. Lim, J. Liu, and A. Ardavan, Fault-tolerant qubit encoding using a spin-$7/2$ qudit, Phys. Rev. A **108**, 062403 (2023).

[45] See Supplemental Material at http://link.aps.org/supplemental/10.1103/PhysRevLett.134.070603 for details of experimental setup, pulse sequences and spectroscopic data.

[46] A. J. Sigillito, A. M. Tyryshkin, T. Schenkel, A. A. Houck, and S. A. Lyon, All-electric control of donor nuclear spin qubits in silicon, Nat. Nanotechnol. **12**, 958 (2017).

[47] S. Omanakuttan, A. Mitra, M. J. Martin, and I. H. Deutsch, Quantum optimal control of ten-level nuclear spin qudits in Sr87, Phys. Rev. A **104**, 060401 (2021).

[48] A. Ruskuc, C.-J. Wu, J. Rochman, J. Choi, and A. Faraon, Nuclear spin-wave quantum register for a solid-state qubit, Nature (London) **602**, 408 (2022).

[49] A. Hausmann and H. Huppertz, Paramagnetic resonance of ZnO∶Mn + + single crystals, J. Phys. Chem. Solids **29**, 1369 (1968).

[50] R. E. George, J. P. Edwards, and A. Ardavan, Coherent spin control by electrical manipulation of the magnetic anisotropy, Phys. Rev. Lett. **110**, 027601 (2013).

[51] R. Böttcher, A. Pöppl, M. Lorenz, S. Friedländer, D. Spemann, and M. Grundmann, 55Mn pulsed ENDOR spectroscopy of Mn2+ ions in ZnO thin films and single crystal, J. Magn. Reson. **245**, 79 (2014).

[52] E. Knill, I. Chuang, and R. Laflamme, Effective pure states for bulk quantum computation, Phys. Rev. A **57**, 3348 (1998).

[53] E. Knill, R. Laflamme, R. Martinez, and C.-H. Tseng, An algorithmic benchmark for quantum information processing, Nature (London) **404**, 368 (2000).

[54] R. M. Brown, A. M. Tyryshkin, K. Porfyrakis, E. M. Gauger, B. W. Lovett, A. Ardavan, S. Lyon, G. A. Briggs, and J. J. L. Morton, Coherent state transfer between an electron and nuclear spin in N15@C60, Phys. Rev. Lett. **106**, 110504 (2011).

[55] G. Wolfowicz, H. Maier-Flaig, R. Marino, A. Ferrier, H. Vezin, J. J. L. Morton, and P. Goldner, Coherent storage of microwave excitations in rare-earth nuclear spins, Phys. Rev. Lett. **114**, 170503 (2015).

[56] J. J. L. Morton, A. M. Tyryshkin, A. Ardavan, K. Porfyrakis, S. A. Lyon, and G. A. D. Briggs, Measuring errors in single-qubit rotations by pulsed electron paramagnetic resonance, Phys. Rev. A **71**, 012332 (2005).

[57] N. V. Vitanov, Dynamical rephasing of ensembles of qudits, Phys. Rev. A **92**, 022314 (2015).